Time-Based GPS Trajectory Guidance

Matt Jardin, *NASA Ames Research Center*
Sundeep Bajikar, *Intel Corporation*
Jorge Heraud, *Trimble Navigation Ltd.*

BIOGRAPHY

Matt Jardin is an aerospace engineer in the Automation Concepts Research Branch at the NASA Ames Research Center. He is a Ph.D. Candidate in Aeronautics and Astronautics at Stanford University and is working on optimal air traffic control research.

Sundeep Bajikar is a Component Design Engineer at Intel Corporation. He is researching semiconductor product development for providing ubiquitous differential GPS solutions for automotive control and driver assistive display systems.

Jorge Heraud is a senior design engineer in the Mobile Positioning and Communications Group at Trimble Navigation Ltd. He is currently working on integrating GPS with wireless communications devices for vehicle tracking applications.

ABSTRACT

Using the Global Positioning System (GPS) standard positioning service as a navigation sensor, a time-based trajectory guidance system is developed. For demonstration purposes, a 2-dimensional (along-track and time) automobile guidance system is analyzed. Time-based trajectory guidance is achieved by using a GPS-driven real-time display to show the vehicle navigator the error between a baseline trajectory and the current vehicle position. The vehicle pilot is then directed to increase or decrease speed such that the baseline trajectory is followed precisely as a function of time. For the automobile guidance demonstration, a baseline trajectory was created by driving along a highway for about thirty minutes while making occasional speed changes and collecting raw GPS measurements. Simultaneously, GPS measurements were collected at a surveyed reference location so that carrier-aided differential GPS post-processing could be applied to the data to develop a very accurate baseline trajectory. The data runs then used carrier aided stand-alone GPS to create a display in the car to show the navigator the along-track position error between the baseline trajectory and the current trajectory in real-time. The driver was directed by the navigator to change speed as required to keep the position error as small as practical. The use of a velocity display was also investigated. Using these displays, the measured final time error at the end of the nominally thirty-minute baseline trajectory was less than the estimated 3σ value of seven seconds in both real-time experimental runs. Some discussion is presented regarding the potential for applying time-based guidance to other vehicles, including general-aviation aircraft, trains, and ships.

INTRODUCTION

The goal of this experiment was to demonstrate the ability to achieve time-based trajectory guidance using an inexpensive stand-alone GPS receiver for navigation. The two primary applications that inspired this experiment were in the area of enhanced cruise-control systems for automobiles and enhanced flight-management capabilities for general-aviation aircraft. Applications in other areas such as train schedule following and cargo ship schedule following may also be improved by the technology demonstrated in this report. The 2-dimensional (longitudinal position and time) guidance experiment described in this paper is a simplified version of more general 3-dimensional (3D) guidance (two surface spatial dimensions and time) and 4-dimensional (4D) guidance (three spatial dimensions and time) for use in ground, air, or sea vehicle applications. Although real-time differential GPS (DGPS) was not demonstrated in this experiment, the use of differential corrections would simply result in reduced tracking error variances by removing the effects of selective availability and other errors.

A time-based trajectory tracking system using Differential GPS (DGPS) position estimation could find several applications in the field of Intelligent Transportation Systems (ITS). For example, with centimeter level

positioning accuracies provided by onboard DGPS [1], it is possible to implement an "Adaptive Cruise Control System" (ACCS) for the consumer automobile market. The ACCS would receive driver input on the required destination and would then select the most appropriate time-based trajectory among the ones available through its onboard database for that destination. In addition to basic map based navigation, the trajectory selection criteria would include the time of the day and real-time traffic conditions available over a mobile data-link. The ACCS would then program itself to follow the identified time-based trajectory towards the specified destination, using the onboard DGPS system as the primary means of positioning. The human driver would still be responsible for vehicle operation and collision avoidance.

The tracking of time-based trajectories has also been of great interest to the air transportation industry where operating costs are a function of both the speed at which trajectories are followed and of the ability to meet arrival/departure schedules [2,3,4]. The constraint that each air vehicle must remain separated from one another also motivates the need for precise trajectory tracking capabilities. As the air traffic control systems of the world move towards time-based regulation, general aviation aircraft will also need to be equipped with time-based regulation capabilities in order to blend in with the more dominant commercial aircraft operations. The GPS holds promise for providing sophisticated time-based control to general aviation aircraft at a very low cost.

To demonstrate time-based vehicle guidance, an automobile was to be guided along a baseline trajectory consisting of position coordinates as a function of time. This experiment would show that the automobile could be caused to track position as a function of time in order to arrive at a final position at a predicted final time. For the automobile guidance demonstration, a baseline trajectory was created by driving along a highway for about thirty minutes while making occasional speed changes of about five or ten miles per hour and collecting raw GPS measurements. Simultaneously, GPS measurements were collected at a surveyed reference location so that carrier-aided differential GPS post-processing could be applied to the data to develop a more accurate baseline trajectory than could be achieved with stand-alone GPS. The data runs then used carrier aided stand-alone GPS to create a display in the car to show the navigator the along-track position error between the baseline trajectory and the current trajectory in real-time. The driver was directed by the navigator to change speed as required to keep the position error as small as practical. Using these displays, the measured final time error at the end of the nominally thirty-minute baseline trajectory was less than the estimated 3σ value of seven seconds in both cases.

This experiment involves two parts: 1) The recording and data-smoothing of two baseline trajectories, and 2) the real-time trajectory tracking runs. The baseline trajectory recording and processing will be discussed first, followed by discussion of the real-time trajectory tracking runs. This report will conclude with a presentation of the results of the trajectory tracking experiments.

BASELINE TRAJECTORY RECORDING AND PROCESSING

The experiments were performed on a stretch of Interstate Highway 280 (I-280) between Los Altos and Daly City, California. The baseline data for the northbound run were recorded starting at GPS time-of-week 105246 on 5/23/99 by driving from just before the El Monte Rd. on-ramp of northbound I-280 to the large Pacifica exit sign that extends over the roadway, ending at GPS time-of-week 107065.5. The baseline data for the southbound run were recorded starting at GPS time-of-week 107493 (also on 5/23/99) by driving from a Daly City on-ramp of southbound I-280 to the "El Monte 1-1/4 mi." sign, ending at GPS time-of-week 109230. During each of the runs, several speed changes were made, and lane changes were made as required to pass slower vehicles. These runs occurred late on a Sunday night so that the highway would be relatively free of traffic. The Garmin GPS 35 PC receiver/antenna was mounted on the driver's side of the dashboard and connected to a 150 MHz Intel Pentium multimedia notebook computer. Raw pseudorange measurements were collected in the vehicle at the rate of 1 Hz.

The position solutions for the baseline runs were computed from the raw pseudorange measurements in post-processing. Four solutions were generated for the purpose of algorithm comparison: 1) Stand-alone GPS, 2) Carrier-aided Stand-alone GPS, 3) Differential GPS, and 4) Carrier-aided Differential GPS. The carrier aided differential solution showed the lowest measurement variance (as expected) and was therefore used to create the baseline run data. Some of these error statistics are presented later in this report.

Carrier smoothing was employed for two main reasons: 1) to reduce errors due to temporally-decorrelated errors (e.g. multipath) in both the baseline and tracking runs, and 2) to improve velocity measurements for use in the tracking runs. The use of carrier smoothing has been well documented in the literature as a very effective way to achieve these two goals [5, 6, 7].

Smoothed pseudoranges for a given satellite and user (superscript k and subscript u omitted) are computed using the following equation

$$\hat{\rho}(t_j) = \frac{1}{L}\tau(t_j) + \frac{(L-1)}{L}(\hat{\rho}(t_{j-1}) + (\phi(t_j) - \phi(t_{j-1}))) \quad (1)$$

where $\hat{\rho}$ is the smoothed pseudorange, L is the length of the filter, τ is the raw code-phase pseudorange, and ϕ is the raw carrier-phase pseudorange (with any integer ambiguity included). The carrier-phase pseudorange is formed from the raw data by summing together the fractional wavelength and the number of whole integer wavelengths as reported by the receiver.

For smoothing stand-alone pseudorange measurements, Eq. 1 may be applied directly. For smoothing differential corrected pseudorange measurements, Eq. 1 is applied with τ replaced by the differential-corrected pseudorange and ϕ is replaced by the differential-corrected carrier-phase pseudorange (again, with any integer ambiguity included).

When the cycle slip indicator from the GPS receiver is non-zero, the carrier-phase measurements have very likely skipped some integer number of carrier wavelengths so that the differencing of carrier-phase measurements should not be used. In all of the carrier smoothing applications in this report, when a cycle slip was detected, the filter was reset by setting $\hat{\rho}(t_j) = \tau(t_j)$. At epochs for which this happens, the smoothed pseudorange measurements might be discontinuous.

Since the baseline data were being post-processed, the position solutions could be further smoothed to help reduce the baseline error for the real-time runs. For epochs where too few satellites were in view for a position solution, the positions were filled in by linearly interpolating the nearest two points before and after the missing epoch. The few remaining spikes in the data that were caused by outliers were also filled in by linear interpolation. The outliers were identified by limiting the change in position from one epoch to the next by an amount equivalent to the approximately-known car velocity. After this filtering, the baseline trajectory was quite smooth and provided a good reference to follow during the data collection runs (Fig. 1).

The velocity and heading for the baseline runs had to be computed using finite differencing between neighboring points and was still too noisy to use so that further filtering was required. This was accomplished by designing a simple Kalman Filter that could also be used during the real-time data runs. The noise covariance matrix for the filter was determined by calculating the variance of the stand-alone carrier aided finite-difference velocity and position. Some outliers were removed prior to filtering if they were above or below certain physical velocity threshold values. The standard deviation of the velocity was $\sigma_v = 4.6$ meters per second. The standard deviation of the heading measurements was more difficult to estimate because the heading really did vary significantly during the baseline run. Therefore, for the filter design, a nominal noise covariance was set and the corresponding process

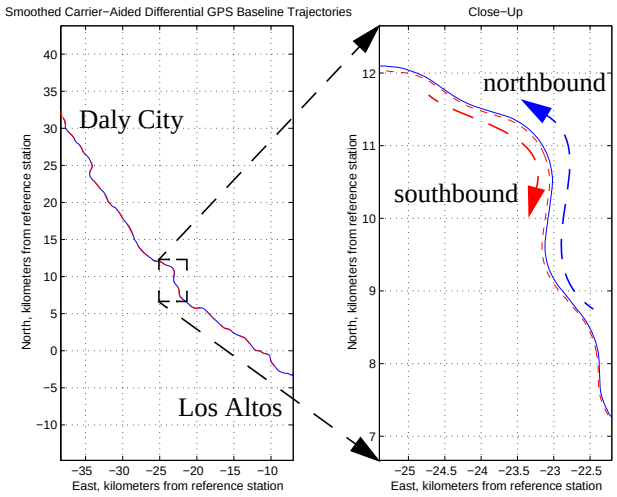

Figure 1. Plots of the baseline trajectory from differential carrier-aided GPS after additional smoothing. Notice that in the close-up plot, the separation of the southbound and northbound trajectories becomes evident.

noise was varied until a nice filter response was obtained that was neither too slow nor too noisy. The dynamic model used for the filter design was

$$\begin{bmatrix} \dot{V} \\ \dot{V}_c \\ \dot{\psi} \\ \dot{\psi}_c \end{bmatrix} = \begin{bmatrix} -0.2 & 0.2 & 0 & 0 \\ 0 & 0 & 0 & 0 \\ 0 & 0 & -0.2 & 0.2 \\ 0 & 0 & 0 & 0 \end{bmatrix} \begin{bmatrix} V \\ V_c \\ \psi \\ \psi_c \end{bmatrix} \qquad (2)$$

$$\begin{bmatrix} V \\ \psi \end{bmatrix} = \begin{bmatrix} 1 & 0 & 0 & 0 \\ 0 & 0 & 1 & 0 \end{bmatrix} \begin{bmatrix} V \\ V_c \\ \psi \\ \psi_c \end{bmatrix}$$

where two bias states were augmented to the first-order lag dynamics for the velocity and heading so that the filter could follow bias values. The units in the dynamic model are meters per second and radians per second. The dynamic model in Eq. 2 was discretized at 1 Hz using a zero-order hold discretization, and the resulting linear quadratic esti-

mator (LQE) was implemented by the following sets of equations

$$\begin{bmatrix} \hat{V}(k) \\ \hat{\psi}(k) \end{bmatrix} = \begin{bmatrix} 0.751 & 0 & 0 & 0 \\ 0 & 0 & 0.578 & 0 \end{bmatrix} \begin{bmatrix} \bar{x}_1(k) \\ \bar{x}_2(k) \\ \bar{x}_3(k) \\ \bar{x}_4(k) \end{bmatrix} + \begin{bmatrix} 0.249 & 0 \\ 0 & 0.422 \end{bmatrix} \begin{bmatrix} V_m(k) \\ \psi_m(k) \end{bmatrix} \quad (3)$$

$$\begin{bmatrix} \bar{x}_1(k+1) \\ \bar{x}_2(k+1) \\ \bar{x}_3(k+1) \\ \bar{x}_4(k+1) \end{bmatrix} = \begin{bmatrix} 0.538 & 0.181 & 0 & 0 \\ -0.423 & 1 & 0 & 0 \\ 0 & 0 & 0.298 & 0.181 \\ 0 & 0 & -0.967 & 1 \end{bmatrix} \begin{bmatrix} \bar{x}_1(k) \\ \bar{x}_2(k) \\ \bar{x}_3(k) \\ \bar{x}_4(k) \end{bmatrix} + \begin{bmatrix} 0.281 & 0 \\ 0.423 & 0 \\ 0 & 0.521 \\ 0 & 0.967 \end{bmatrix} \begin{bmatrix} V_m(k) \\ \psi_m(k) \end{bmatrix} \quad (4)$$

where the measured velocity (V_m) and measured heading angle (ψ_m) are functions of the time-difference of the East (E), North (N), and Up (U) components and are computed as

$$V_m(k) = \frac{\sqrt{\Delta E(k)^2 + \Delta N(k)^2 + \Delta U(k)^2}}{\Delta t(k)} \quad (5)$$

and

$$\psi_m(k) = \text{atan}2(\Delta E(k), \Delta N(k)) \quad (6)$$

where, for any variable A,

$$\Delta A(k) \equiv A(k) - A(k-1) \quad (7)$$

As can be seen, the filtered velocity (Fig. 2) and heading (Fig. 3) are much improved over the raw differenced measurements. The spikes in the raw and filtered measurements are due to typical stand-alone GPS position error sources such as multi-path and dropped satellite signals. Note that the maximum velocity spikes are at 80 miles per hour due to the action of a simple logic pre-filter which did not allow velocity measurements to go above this value for physical reasons.

The processed baseline run data were written to a file for use in the real-time data runs. The baseline data consisted of time, East position, North position, Up position, heading angle, and velocity.

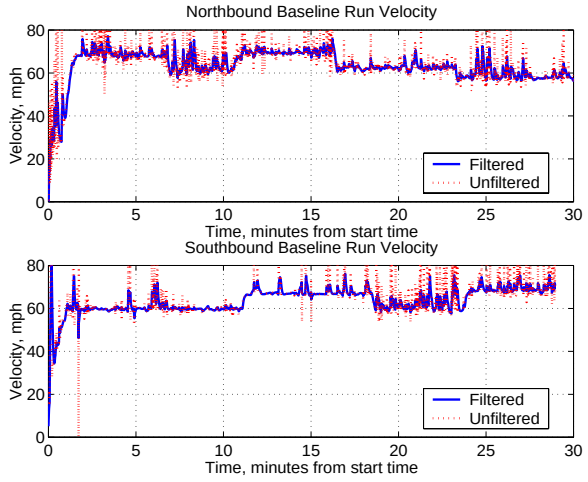

Figure 2. The Kalman-Filtered velocity profiles for both the southbound and baseline runs show improvement over the raw measurements without noticeably slowing down the velocity measurement response. Note that the step speed changes are readily visible.

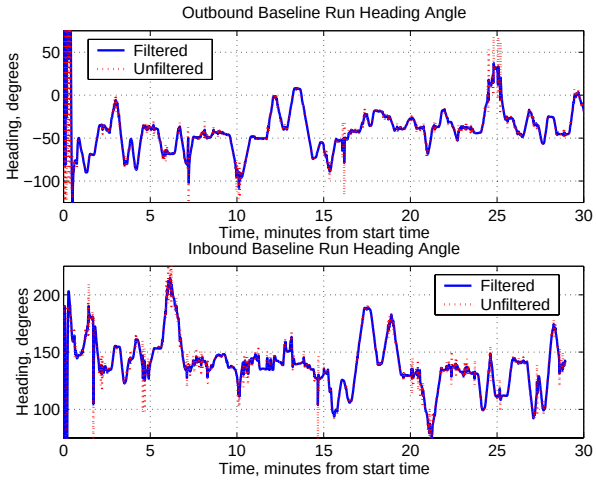

Figure 3. The Kalman-Filtered heading-angle profiles for both the southbound and baseline runs show improvement over the raw measurements without noticeably slowing down the measurement response. Note that the southbound and northbound heading plots are roughly mirror images of one another about the vertical axis and are 180º different.

DIFFERENTIAL REFERENCE STATION

As mentioned previously, Differential GPS was used to post-process the baseline trajectory data. Two receivers were used to implement DGPS, and a third one was used to validate the differential corrections.

The reference receiver was located at the intersection of North Mary Avenue and Maude Avenue in Sunnyvale on top of the Trimble sign that has a brass ball and a surveyed value for the Latitude and Longitude (37degree, 23 minutes, 32.270 seconds North and 122 degrees, 02 minutes and 16.139 seconds). This provided a differential GPS baseline distance of about 8.5 km. As will be discussed later, the datum used for these measurements was not known so that some error could result from the difference between this datum and WGS84. The receiver/antenna was mounted on top of a 4x4 wood pole 1 meter high. The altitude for the reference receiver was obtained by averaging the collected data. Assuming that the given latitude and longitude for the reference station were relative to the WGS84 datum, the WGS84 XYZ coordinates were computed to be $XYZ = \begin{bmatrix} -2691469.777 & -4300932.716 & 3852064.685 \end{bmatrix}^T$. The reference station had a clear view of the horizon to at least 5 degrees of elevation in all directions except North where the minimum visible elevation was 10 degrees.

The differential corrections were applied as pseudorange corrections computed at the reference station as recommended in the literature [5]. This approach was preferred because it would provide direct position solutions for the rover as opposed to the position of the rover relative to the reference station, and because it would be more straightforward to match satellite data to both the reference station and the two rovers. The pseudorange correction was calculated at the reference station by subtracting the calculated range to the satellite (satellite position at time of transmission - known position) minus the pseudorange as reported by the receiver as follows

$$\begin{aligned} \Delta\rho_{ref}^{(k)} &= \left| r_{ref} - r^{(k)} \right| - \rho_{ref}^{(k)} \\ &= -b_{ref} + B^{(k)} - I_{ref}^{(k)} - T_{ref}^{(k)} - \nu_{ref}^{(k)} \end{aligned} \tag{8}$$

Corrections for the ionosphere, troposphere, and the satellite clock were not applied at either the reference or the two rovers because these terms would cancel out when the pseudorange corrections were applied to the rover-measured pseudoranges. At the rovers, the correction from Eq. 8 was applied to the pseudorange reported by the receiver. This created a new set of corrected pseudoranges for the rover. These corrected pseudo ranges were then used to calculate the position of the rover. The corrected pseudorange at the rover was then given by

$$\begin{aligned} \rho_{cor} = \left| r_{rov} - r^{(k)} \right| + b_{ref,rov} - B_{ref,rov}^{(k)} + \\ I_{ref,rov}^{(k)} + T_{ref,rov}^{(k)} + \nu_{ref,rov}^{(k)} \end{aligned} \tag{9}$$

where the errors due to ionosphere, troposphere, and satellite clock error mostly canceled as long as the corrections were applied without too much time delay and the rover was not too far from the reference station (less than 100 km or so).

As in stand-alone mode, one must solve for the receiver clock error. In this case, this is the difference between the reference clock error and the rover clock error ($b_{ref,rov} = b_{rov} - b_{ref}$). Solving for this difference in clock errors is straightforward, but one must be careful not to mix together corrected and uncorrected measurements unless the rover clock error is solved for independently. Another critical point is that differential corrections from different satellites *must have been measured at the same time.* Rather than complicate the differential correction algorithms, the decision was made to use only corrections from the same epoch, and to use only those pseudorange measurements for which corrections were available. One other subtle point is that at the rover, the uncorrected pseudorange must be used to compute the time-of-transmission for each satellite.

A plot of the stand-alone GPS position solution at the reference station demonstrates that there was a bias position error in the surveyed latitude and longitude coordinates relative to the WGS84 datum (Fig. 4). The

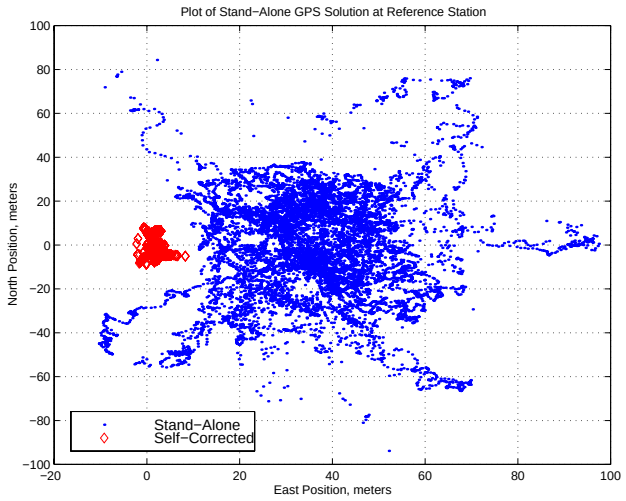

Figure 4. The Stand-Alone GPS solution at the reference station shows that there is a bias in the surveyed reference station location relative to the WGS84 datum.

mean position errors were computed to be 36.15m, -0.622m, and 13.0m in the East, North, and Up directions respectively. This bias was be subtracted from the baseline data so that the stand-alone solutions would match up with the baseline trajectory more closely during the real-time runs.

When the differential corrections were applied to the reference station data, the resulting position should have equaled the surveyed coordinates to within numerical precision of the computer. Any error sources should have been canceled out in the process of computing a correction, and then backwards computing the theoretical range to each satellite. However, an undetermined error was present

in the data such that the differential-corrected solution had a standard deviation of approximately 9 meters. The suspected reason is that the time-stamps of the differential corrections were not accurate. Since this error was present in the baseline trajectory data, this additional position variance was present while trying to track the reference trajectory in real-time. This will be addressed further in the error-budget analysis for the real-time system.

A validation rover, ROV_0, was located exactly 8 meters away from the reference station atop another wooden pole, and 1 meter lower than the reference station. ROV_0 was static during the experiment and was set it up for the purpose of directly measuring the accuracy of the differential GPS system. The differential corrected ROV_0 solutions exhibit the same standard deviation of approximately 9 meters as was seen in the self-corrected reference station solutions (Fig. 5). Also evident is the bias

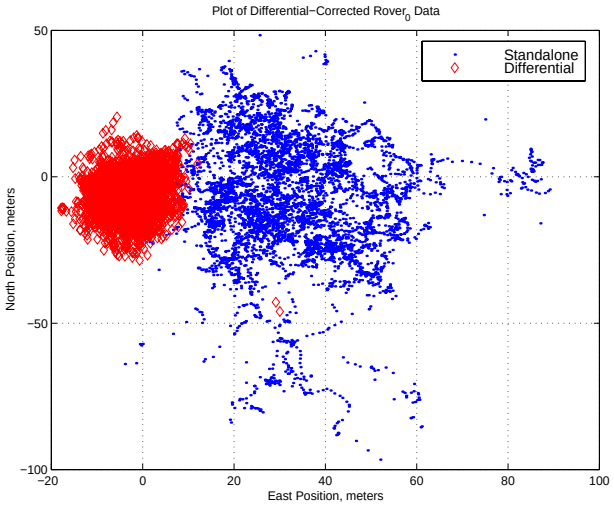

Figure 5. The differential-corrected ROV_0 data were used to validate that the differential corrections were improving the solution accuracy.

error in the stand-alone position solution. The standard deviation of the differential-corrected position solution error was expected to be in the sub-meter range. For the purpose of real-time trajectory tracking, a standard deviation on the order of 10 meters does not present a problem.

The pertinent Dilution of Precision values (DOPs) at the reference station, the ROV_0 station, and the remote car station have been calculated and are tabulated in Table 1. In addition to the DOPs, the statistics of the position errors for the reference station have been computed and tabulated in Table 2.

Table 1: Dilution of Precision (DOPS)

Station and Algorithm	mean HDOP	mean VDOP	mean # of Satellites	Time (sec)
Reference Station	0.97	2.57	6.68	9519
ROV_0	0.75	3.99	6.68	3242
Stand Alone Baseline Run1	1.81	4.94	5.85	1819
Differential Baseline Run1	1.82	5.00	5.82	1819
Stand Alone Baseline Run2	1.37	3.32	6.32	1737
Differential Baseline Run2	N/A	N/A	N/A	1737

Table 2: Position Error Statistics

Station	Statistic	σ_{east} meters	σ_{north} meters	σ_{up} meters
Reference Station	Stand Alone	15.6	23.5	55.2
Reference Station	Carrier Aided Stand Alone	15.55	23.54	54.95
Baseline Run1	Stand Alone minus Carrier Aided Differential	19.20	132.01	122.02

Table 2: Position Error Statistics

Station	Statistic	σ_{east} meters	σ_{north} meters	σ_{up} meters
Baseline Run1	Difference between Carrier Aided Stand Alone and Carrier Aided Differential	19.10	128.5	119.24
Baseline Run2	Difference between Stand Alone and Carrier Aided Differential	32.86	29.14	123.7
Baseline Run2	Difference between Carrier Aided Stand Alone and Carrier Aided Differential	34.9	31.5	129.9

REAL-TIME TRAJECTORY TRACKING RUNS

A Garmin GPS 35 PC receiver and a 150 MHz Intel Pentium multimedia notebook computer were used for the real-time experiments. The GPS receiver was connected to the COM 1 serial port of the notebook computer. The serial data acquisition routine was augmented with a Matlab MEX interface (gateway) function, and compiled as a MEX DLL on Matlab 5.0 Student Edition, running on the notebook computer. The C-language compiler used was Microsoft Visual C++ 5.0.

The on-board computer on the test vehicle (a 1998 BMW M3 sedan) was used as the reference source for velocity measurement. The car's on-board computer provided a well calibrated digital reading of the instantaneous velocity. This measurement was used to complement the analog speedometer in adjusting the speed of the car in accordance with the experiment design.

The position tracking display was configured to always be centered on the current position and showed along-track and cross-track position error (Fig. 6). Since the heading measurements from stand-alone GPS measurements were shown to be quite noisy during the processing of the baseline run, the East and North position errors were

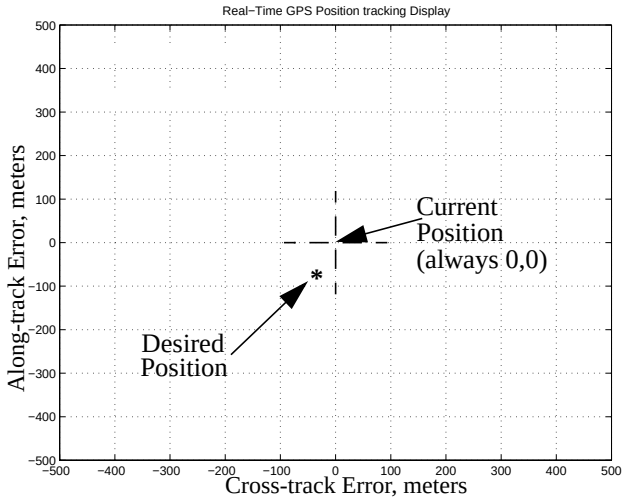

Figure 6. The along-track and cross-track position error display used during the real-time trajectory tracking runs.

rotated to the baseline along-track and cross-track reference frame by using the smoothed heading data from the baseline run. As long as the position error was kept small (less than 100 meters), the baseline along-track and cross-track frame would provide an excellent estimate of the true current heading. As the position error was driven to zero, the baseline along-track and cross-track frame would align exactly with the current frame. This worked extremely well.

The measured position error was also run through a simple Kalman Filter similar to the one used to filter the velocity. The filter equations are given by

$$\begin{aligned} \Delta\hat{x}(k) &= 0.8239\bar{x}(k) + 0.080933\Delta x_m(k) \\ \bar{x}(k+1) &= 0.91055\bar{x}(k) + 0.08945\Delta x_m(k) \end{aligned} \tag{10}$$

Identical decoupled filters were used for both the along-track and cross-track directions. The units for this filter were meters, and the sample rate was 1 Hz.

A marker (asterisk in Fig. 6) indicated the desired position at the current time. If the desired position was ahead of the current position, the speed of the car was increased to make the desired position marker coincide with the current position (center of the display). Similarly, if the desired position was behind the current position, the speed of the car was reduced to track the desired position. The navigator sitting in the passenger seat with the notebook computer viewed the display and relayed commands to the driver as necessary to keep the position error small. A simple text display of the current velocity as measured by GPS was also employed to try and give some lead information to the navigator. The algorithm flowchart for the real-time system appears in Fig. 7.

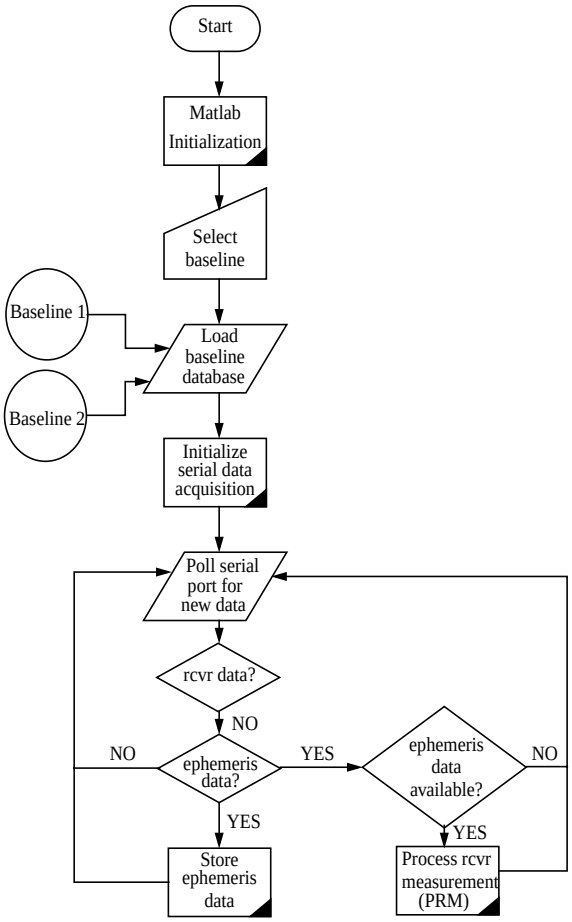

Figure 7. Flowcharts of real-time algorithms for the trajectory tracking runs.

RESULTS

The expected guidance accuracy can be estimated by accounting for the various sources of errors involved. The main error sources are baseline trajectory error, real-time navigation error, real-time driving technical error, and real-time latency error. Latency error may come from receiver delay, serial communication delay, operating system delay, and computation delay in generating the error display. Ignoring latency errors for the moment, and assuming that the other errors are independent, the total variance for trajectory tracking, σ_{tot}^2, is given by the sum of the baseline variance, σ_{bas}^2, the navigation variance, σ_{nav}^2, and the driving technical error variance, σ_{dte}^2

$$\sigma_{tot}^2 = \sigma_{bas}^2 + \sigma_{nav}^2 + \sigma_{dte}^2 \qquad (11)$$

This expression (Eq. 11) can be used to estimate the total error variance prior to driving. The along-track error variance for driving technical error depends upon how much effort the driver and navigator are willing to expend to keep the car on track. After a few trial runs, it was determined that keeping the position error less than 120 meters was feasible for a manually controlled vehicle. If 120 meters is considered to be the 2σ value for the driving technical error distribution, then the error variance is 60 meters squared. The baseline along-track error variance can be approximated based on the measured error variances at ROV_0 of about 10 meters squared. The navigation error can be approximated based on the measured error variance at the receiver for the stand-alone GPS solution of about 20 meters squared. When added together, and the square root is taken, the standard deviation of the total position error for the driving runs is expected to be about 65 meters. The total error is obviously dominated by driving technical error. Assuming a Gaussian error distribution, one would expect that 99% of all trajectory tracking runs should be within about 3σ, or ± 195 meters, of the baseline trajectory. Equivalently, at a nominal speed of 28 m/s, this corresponds to a time error of about ± 7 seconds.

During the two trajectory tracking runs, the mean and standard deviation of the difference between the measured positions and the baseline positions were measured (Tables 3 and 4). Also shown in these tables are the final time errors at the final-position landmarks. These values were obtained by using an independent timepiece to measure the time at the final position landmarks. The measured values were then compared to the baseline values. These two data runs show that the measured error standard deviations are both very close to the estimated value of 65 meters. The final

Table 3: Run 1 Measured Error Statistics

Statistic	Cross-Track	Along-Track
Mean	7.95 m	-15.43 m
Standard Deviation	23.94 m	59.46 m
Independently Measured Final Time Error	N/A	6.5 sec

Table 4: Run 2 Measured Error Statistics

Statistic	Cross-Track	Along-Track
Mean	10.38 m	2.07 m
Standard Deviation	28.29 m	55.15 m
Independently Measured Final Time Error	N/A	0 sec

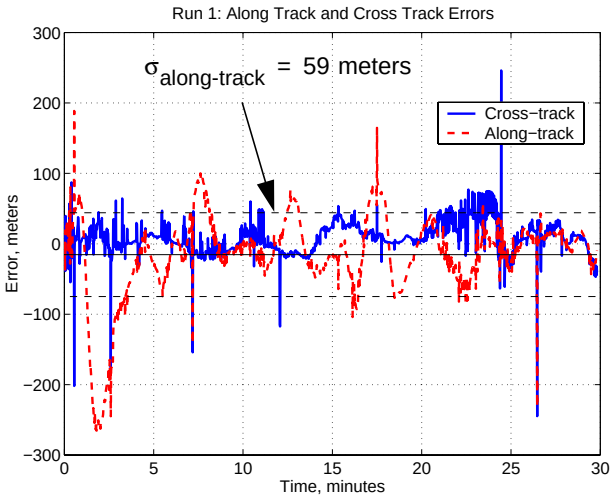

Figure 8. The along-track and cross-track position errors for tracking run 1.

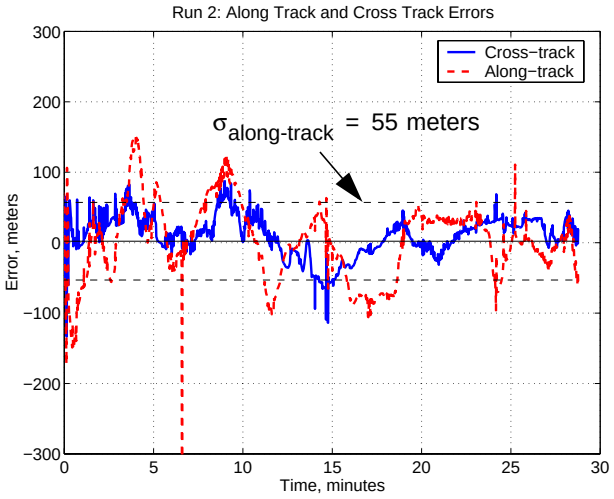

Figure 9. The along-track and cross-track position errors for tracking run 2.

time errors are also within the estimated 3σ value of seven seconds. The plots of the along-track and cross-track errors (Figs. 8 & 9) show how the runs progressed. Notice that the cross-track error variance is much smaller than the along-track error variance since the car was physically constrained to follow the lanes of the roadway and was unaffected by driving technical error.

CONCLUSIONS

By using a real-time display with carrier aided stand-alone GPS position measurements, a car was guided along a baseline trajectory to arrive at a point approximately 50 km away to within seven seconds of the desired time. With additional work to create a better real-time display, a real-time differential data-link, and modifications for different vehicle dynamics, the results of this experiment could be readily applied to the 4-dimensional aircraft trajectory tracking problem. The applications for which this experiment will be useful are those of enhanced automobile cruise control systems, general aviation flight management systems, and maritime scheduling systems.

ACKNOWLEDGEMENTS

The authors wish to thank Keith Alter of Stanford University for his helpful advice in this research experiment.

REFERENCES

[1] Bajikar, S., Gorjestani, A., Simpkins, P., and Donath, M., “Evaluation of In-Vehicle GPS Based Lane Position Sensing for preventing Road Departure”, Proceedings of the IEEE Conference on Intelligent Transportation Systems, ITSC ’97, Boston, MA, 1997.

[2] Braff, R., Powell, J.D., and Dorfler, J., “Applications of the GPS to Air Traffic Control,” *Global Positioning System Theory and Applications, Volume II*, AIAA, 370 L’Enfant Promenade, SW, Washington, DC, 1996, pp. 327-374.

[3] Erzberger, H., and Pescavaradi, T., “4-D Guidance System Design with Application to STOL Air Traffic Control,” AIAA Paper A72-38252, 13th Joint Automatic Control Conference, Stanford, CA, Aug. 16-18, 1972.

[4] Erwin Jr., R.L., “‘Strategic’ Time-Based ATC,” *Astronautics and Aeronautics*, v. 16, n. 11, Nov. 1978, pp. 56-61.

[5] Parkinson, B.W., and Enge, P.K., “Differential GPS,” *Global Positioning System Theory and Applications, Volume II*, AIAA, 370 L’Enfant Promenade, SW, Washington, DC, 1996, pp. 3-50.

[6] Misra, P., Burke, B.P., and Pratt, M.M., “GPS Performance in Navigation,” *Proceedings of the IEEE*, Vol. 87, No. 1, Jan., 1999, pp. 65-85.

[7] Enge, P., “Local Area Augmentation of GPS for the Precision Approach of Aircraft,” *Proceedings of the IEEE*, Vol. 87, No. 1, Jan., 1999, pp. 111-144.